# MOTION CHARACTERISTICS OF A REVERSE THRUST ADSORPTION WALL-CLIMBING ROBOT WITH MULTI-DEGREE-OF-FREEDOM PROPELLER

Minglu Chi,* Shuaibing Chang,** Fuchao Yang,* Xiaoyan Qian,*** Shuaihua Cui,* Jinzhan Wang,* Lun Zhao,* and Ruihua Ren*

**Abstract**

In this paper, a reverse thrust adsorption wall-climbing robot (WCR) with multi-degree-of-freedom Propeller (WCRMP) is presented, from a design development and experimental evaluation perspective. Two symmetrical propeller discs, placed at the front and the rear side, provide a stable driving force. The left and right control frames, with multiple degrees of freedom, can adjust the position of the propeller head, in the left and right direction and adjust the direction of tension. The static characteristics of the WCRMP on the horizontal plane and on the vertical wall are analysed and the balance relationship, during the transition from the horizontal plane to the vertical wall, is obtained. The aerodynamic characteristics of the reverse thrust adsorption system of the WCRMP are analysed, using the momentum inflow model and the Euler force balance theorem, while the pressure distribution of the twin propellers is measured. When the clearance between the propellers changes, the pressure distribution, in the propeller rotation domain, will also change. The adsorption force, obtained during the rotation of the twin propellers, varies according to the position of the left and right control frames. The adsorption experiments show that the WCRMP can switch freely from the horizontal plane to the vertical wall, maintaining stable adsorption. When the angle between the WCRMP and the ground is 0° and the angle of the head of the front and rear propeller is 90°, the tension reaches the maximum value, which verifies the feasibility of the proposed driving control of the WCRMP. This work demonstrates that the reverse thrust adsorption system may potentially improve the flexibility and stability of WCRMPs.

* School of Intelligent Engineering, Henan Institute of Technology, Xinxiang, China; e-mail: cmlcml86@163.com; {303723877, 2180826663, 3452184163, 480190334, 3590638950}@qq.com
** School of Electrical Engineering and Automation, Henan Institute of Technology, Xinxiang, China; e-mail: zhuadong87@163.com
*** School of Economics, Henan Institute of Technology, Xinxiang, China; e-mail: 1643572566@qq.com
Corresponding author: Shuaibing Chang

*Recommended by Howard Li*
*(DOI: 10.2316/J.2024.206-0947)*

**Key Words**

Wall-climbing robot; multi-degree-of-freedom propeller; movement characteristics; reverse thrust adsorption

## 1. Introduction

Since their emergence in the 1960s [1], wall-climbing robots (WCRs) have been widely used for industrial tasks, like inspection of high-rise constructions, building decontamination, glass exterior wall cleaning, inspections of pipelines cracks, and ship hull detection [2]–[4], especially in dangerous places, where traditional WCRs are hard to access. It is believed that more attractive applications of WCR, such as aircraft photovoltaic (PV) solar panels or fuel tank cleaning, nuclear power facility inspection, and interior space station maintenance, will be realised in the near future, if WCRs with more flexible motion and stable adsorption ability, are developed [5]–[7].

Significant effort has been dedicated to exploring novel adhesion mechanisms, including vacuum or negative pressure suction [8], reverse thrust [9], magnetic adsorption [10], mechanical claws [11], microspine [12], bionic adhesion [13], and tether-supported climbing methods [14], [15], all depending on the material or the shape of the surface. Each method has its advantages and disadvantages.

Vacuum negative pressure adsorption draws out the air in the sucker, through the internal centrifugal fan system, while the air at the bottom of the body is continuously added to the fan system, forming the negative pressure in the cavity. Depending on the pressure difference between atmospheres, pressure is generated and the sucker is pressed on the wall [16]–[18]. This adsorption method is affected, to a great extent, by the roughness of the working surface. In the case of uneven or obstructed wall surface, leaks are easy to occur, resulting in insufficient negative pressure and fall down. Moreover, the vacuum negative pressure adsorption WCR load capacity is not strong.

WCRs that adopt the magnetic adsorption principle will not suffer from air leakage and fall down, so

they are more reliable [19]–[21]. Magnetic adsorption is divided into two types: permanent magnet adsorption and electromagnetic adsorption, which rely on magnetic force adsorption on ferromagnetic wall surface. Permanent magnet adsorption is adsorbed on the wall surface by its own magnetic materials, which has the advantages of simple adsorption structure and large adsorption force. It is mainly used to detect the inner and outer surfaces of large metal vessels. Electromagnetic adsorption uses the principle of electromagnetism, where magnetic attraction adsorption is generated after electrical current generation, whereas the magnetic force is adjusted by changing the current intensity. The generated force is larger than the magnetic force generated by permanent magnet adsorption, but it also requires larger structure and high-power consumption.

Mechanically generated bionic adsorption imitates the characteristics of animal feet adsorbed on a wall surface, which mainly includes dry and humid adsorption [22]–[24]. Moist adhesion uses mucus to adsorb on the wall. There are mainly two forms of dry adsorption: The first form mainly relies on the bristle of the animal's organs for adsorption on wall surface, without involving the secretion of adhesive fluid. The other form of dry adhesion is claw adhesion. Although the bionic adsorption in WCRs shows strong adaptability, its application scope is limited by the research cost of bionic materials and the low load capacity of the robots.

All of these adhesion mechanisms require flat work surface or more complex and large structure to provide enough adsorption force applied on the wall, to drive the WCR on a flexible and reliable motion path. The application of WCRs is limited by stability issues and low load capacity. Since the stable adsorption and simple structure are of primary importance, efficient and highly automated approaches, suitable for WCRs, need to be further developed.

Generally speaking, the reverse thrust adhesion method is more suitable for developing WCRs, due to its reliable adhesion, low cost and low energy requirements. According to the aerodynamic theory, reverse thrust adsorption WCRs use propeller discs or ducted fans, to generate appropriate thrust, to achieve wall adsorption [25]–[27]. A pressure difference is formed, above and below the propeller disc, through the propeller's rotation, which generates relatively stable thrust, so that the WCRs can be reliably adsorbed on the wall. Since the thrust generation device is not in contact with the wall, WCRs do not have high requirements, as regards to the roughness of the wall.

Recently, some research work, on the reverse thrust wall adsorption robots, has been reported. A robot named 'EJBot' was developed by Fanni *et al.* [28], which uses a simultaneous hybrid actuation system, consisting of propeller thrust forces and driving wheel torques. EJBot can climb different kinds of surfaces, like exploring the industrial vessels' interiors, while performing an efficient inspection task. The robot can cross over significant obstacles of 40 mm height. Li *et al.* [29] presented a rotor-propeller type WCR, where the model aircraft propeller is used as the adsorption unit; the rotor platform has two degrees of freedom, one roll and one pitch and the relationship between the wheel and the wall of the WCR is analysed. Wei *et al.* [30] studied the aerodynamics of the propeller. The aerodynamic simulation analysis of the single rotor and the double rotor and the tensile test experiment of the single propeller were carried out. The conclusion was that the aerodynamic forces generated by the two rotors are not linearly superimposed due to the airflow interference, while the rotational speed of the rotors and the distance between the rotor platforms all affect the magnitude of the force. Bhaskar *et al.* [31] presented a wall-climbing bi-copter with dual-axis servo-controlled tilting propellers, where the attitude stabilising control law was constructed according to the PID controller parameters and the motion response was verified using the simulation. It was established that the attitude control algorithm can effectively achieve the attitude stability of the dual rotor aircraft, as required for low speed operations.

All this work has contributed to a better understanding of the adhesion techniques of the WCRs. The analysis of many studies about the WCRs shows that, the existing WCRs generally have problems, such as complicated adsorption mechanism, insufficient adsorption force, weak flexibility and stability on the vertical wall surface, as well as weak load capacity. These issues indicate that the adsorption capacity, the flexibility and the stability are the most important elements.

In this paper, a reverse thrust adsorption WCR with multi-degree-of-freedom propeller (WCRMP) with flexible movement and stable adsorption is designed and tested. The statics and motion characteristics of the WCRMP, on the horizontal plane and on the vertical wall surface, are analysed, while the balance relationship between the movement of the WCRMP, from the horizontal plane to the vertical wall surface, is studied. In order to improve the flexibility of the WCRMP, a propeller disc control frame with multiple degrees of freedom is designed, able to adjust the driving force direction of the WCRMP freely. The aerodynamic characteristics of the WCRMP are analysed. As the clearance between two propellers changes, the pressure distribution in the propeller domain will be directly affected. The tension, generated when the propeller is rotating, will vary, depending on the position of the control frame. The change of inclination angle of the twin propellers will affect the adsorption force of the WCRMP. Experiments show that the WCRMP can switch freely from the horizontal plane to the vertical wall and stable adsorption. At an angle of 0°, between the WCRMP and the ground, while the angle of the head of the front and rear propellers is 90°, the tension reaches the maximum value. This study provides a useful guide to distinguish the required adsorption force for the reverse thrust mechanisms and undertakes the design and optimisation of the WCR.

## 2. Methodology

### 2.1 Structure of a WCRMP

The overall structure of the WCRMP consists of the robot body, propeller head, propeller brushless motor, front wheel

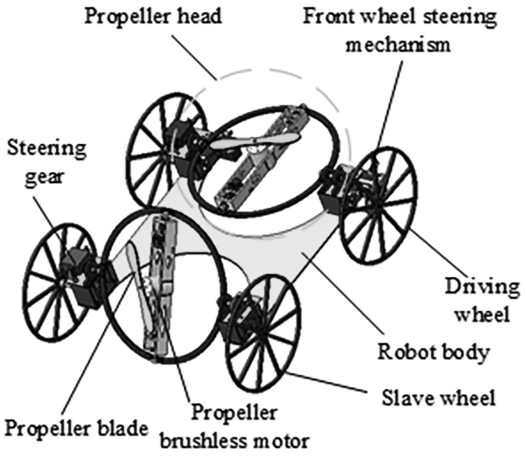


Figure 1. Overall structure of WCRMP.

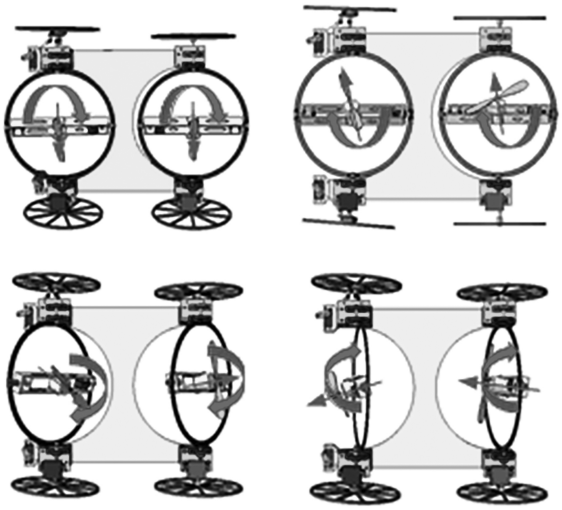

Figure 2. Schematic diagram of propeller head rotation with multiple degrees of freedom.

steering mechanism, steering gear, driving wheel, slave wheel, wireless control module, as shown in Fig. 1.

In order to ensure that the WCRMP can move steadily on the surface of a vertical wall, an oblique downward thrust needs to be generated. Depending on the reaction between the WCRMP and the wall, a pull against gravity is developed. The propeller head of the WCRMP has multiple degrees of freedom and can rotate 180° in four directions, as shown in Fig. 2. The twin propellers head can ensure that, when the tilt angle of the wall surface changes, the thrust can still be adjusted, by adjusting the speed and angle of the double brushless motor, so as to ensure the steady motion of the WCRMP. Brushless motor using electronic commutation instead of mechanical commutation, not only has motor speed performance, but also small size and high efficiency, with good start and timing performance.

### 2.2 Front Wheel Steering Mechanism

The steering mechanism of a WCRMP includes cardan joint, steering gear, RC ball head, and connecting rod. The controller sends signals to the Arduino main control board, to realise the control of the steering gear. The overall control design scheme is shown in Fig. 3.

There is a steering gear on both sides of the front wheel steering structure and steering is realised by driving the connecting rod of the steering gear to drive the hub. The steering mechanism is connected by multiple universal joints, achieving light weight and high turning efficiency, as it can realise fast turning motion on the plane and vertical walls with high stability. The steering gear servos have good speed control ability and anti-load disturbance ability. A 3D schematic diagram of the front wheel steering mechanism is illustrated in Fig. 4.

### 2.3 Principles of Adsorption and Motion of WCRMP

When the WCRMP moves on the horizontal plane and on the surface of the wall, it uses the reverse thrust, generated by two brushless motors, to provide the climbing force. Different motion modes can be realised by adjusting the angle of the front and rear propellers, using the steering gear. As the WCRMP moves from the ground to the wall, it will go through three phases: ground forward, ground to wall movement, and wall climbing. During the transition from the ground to the wall, the front driving system of the WCRMP moves the platform, so as to provide the upward pulling force, while the back driving system provides the forward driving force.

A schematic diagram of steering, driven by the front steering gear of the WCRMP, is shown in Fig. 5. Usually, the motion position of the WCRMP is adjusted by changing the tilt angle of the power shaft, controlled by the front and rear steering engines, followed by the adjustment of the moving process of the WCRMP. At the time, when the WCRMP approaches the wall, the power shaft of the rotor, controlled by the front steering engine, rotates 180°, creating an upward pull, parallel to the climbing wall.

### 2.4 Analysis of Horizontal Plane Motion of WCRMP

Considering the center of the two-wheel hub as the origin, the force coordinates systems $X_1O_1Y_1$ and $X_2O_2Y_2$ of the WCRMPt are established, respectively. The horizontal direction is the $X$-axis and the line normal to the horizontal axis, passing through the origin, is the $Y$-axis. As shown in Fig. 6, the static model of the WCRMP is established. $T_{\mu 1}$ and $T_{\mu 2}$ are the friction forces between the hub and the adsorbed wall. $F_1$ and $F_2$ are the reverse thrust forces, generated by the front and rear brushless motors. The direction of the reverse thrust is parallel to the main shaft of the brushless motors. $\alpha_1$ and $\alpha_2$ are the inclination angles of the front and rear brushless motors, namely, the elevation angle between the rotor of the brushless motors and the WCRMP; $\beta$ is the inclination angle of the WCRMP on the wall; $G$ is the WCRMP's gravity, $r$ is the radius of the hub; $s$ is the wheel pitch; $K_i$ ($i$ = 1, 2, 3, 4) is the pressure exerted by the wall on each wheel.

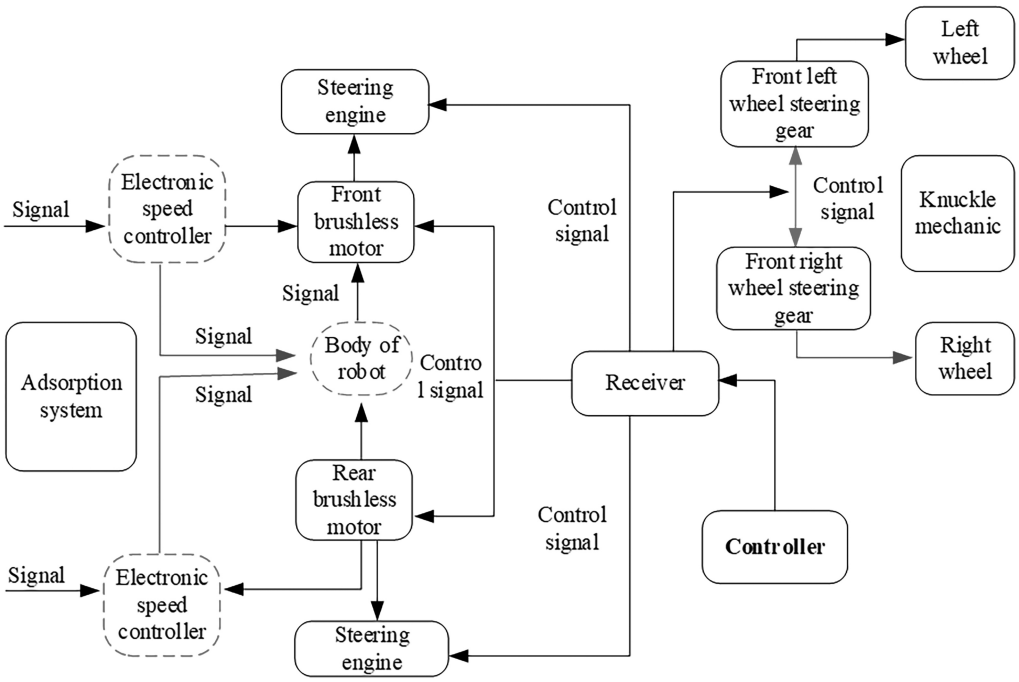


Figure 3. Overall control design of WCRMP.

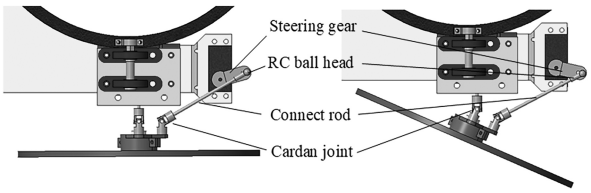


Figure 4. Front wheel steering mechanism.

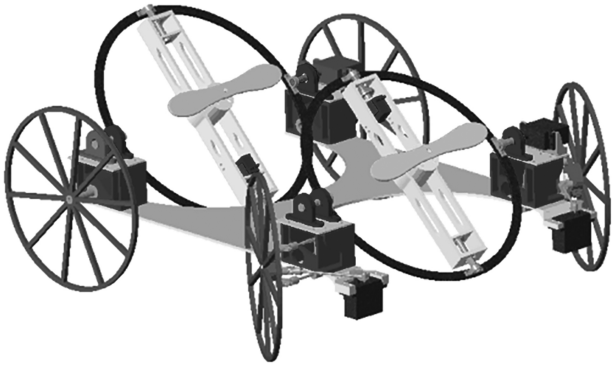

Figure 5. Steering diagram of the WCRMP.

When a WCRMP moves on a horizontal plane, there is the following equilibrium relationship:

$$\left\{\begin{array}{ll} F_1\sin\alpha_1 + F_2\sin\beta - T_{\mu1} - T_{\mu2} & = 0 \\ F_1\cos\alpha_1 + K_1 + K_2 + F_2\cos\beta - G & = 0 \end{array}\right\} \quad (1)$$

As shown in Fig. 7, when the WCRMP moves to the corner and is ready to climb, the relationship is as follows:

$$\left\{\begin{array}{ll} T_{\mu1} + T_{\mu2} - F_N - f - f\sin\beta + F_2\sin\alpha & = 0 \\ K_1 + K_2 + F_1 - G - F_2\cos\alpha - f\cos\beta & = 0 \\ \mathrm{Gc} - sF_2\cos\alpha - \mathrm{fs}\sin\alpha + sK_2 & = 0 \end{array}\right\} \quad (2)$$

Where $\alpha+\beta = \pi/2$, the distance between $O$ and $O_1$ is $c$. The component of $F_2$ moving forward in the horizontal direction is $F_2\sin\alpha$, and the component of $F_2$ moving down in the vertical direction is $F_2\cos\alpha$. $F_N$ is the normal force acting on the wheel, $f$ is the frictional resistance.

As shown in Fig. 8, when the WCRMP has one wheel on the wall and the other wheel on the horizontal plane, it is a critical state:

$$\left\{\begin{array}{ll} F_1\sin\beta_1 - K_1 - F_\tau\sin\alpha_A - f\cos\alpha_A & \\ \quad + T_{\mu2} + F_2\sin\beta_2 & = 0 \\ F_1\cos\beta_1 - T_{\mu1} + F_\tau\cos\alpha_A - f\sin\alpha_A & \\ \quad - G + F_2\cos\beta_2 + K_2 & = 0 \\ F_\tau c + \mathrm{Gc}\sin\phi_2 - sT_{\mu2}\sin\phi_1 & \\ \quad - sF_2\sin(\beta_2 - \phi_2) & = 0 \end{array}\right\} \quad (3)$$

Where $\alpha_A$ is the angle between the WCRMP plane and the horizontal plane, $F_\tau$ is the lift force of the vertical plane of the WCRMP, $\beta_1$ is the inclination angle of the front wheel on the wall, $\beta_2$ is the inclination angle of the rear wheel on the ground, $\varphi_1$ is the angle between the WCRMP rear wheel motion direction and the horizontal plane, and $\varphi_2$ is the angle between the motion direction of the WCRMP front wheel and the vertical plane.

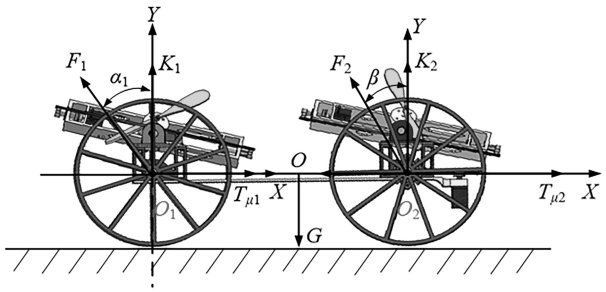


Figure 6. Force balance of the WCRMP in horizontal motion.

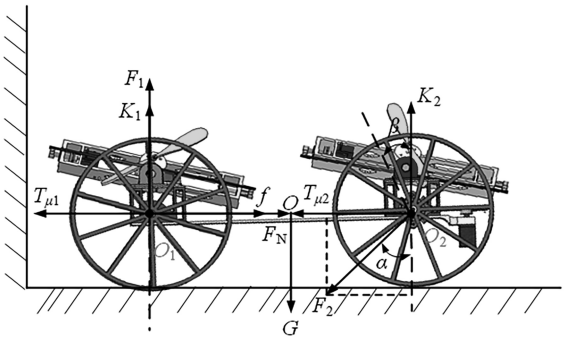


Figure 7. Force balance of the WCRMP in a corner.

### 2.5 Analysis of Climbing Motion of WCRMP

When the WCRMP moves upward on the wall, the overall force situation is shown in Fig. 9.

According to D'Alembert' s principle of virtual work and the force balance relationship, the force equation of the WCRMP, as it moves on the wall, with any posture, is as follows:

$$\begin{cases} K_1 + K_2 - F_1\cos\beta - F_2\cos\alpha_A & = 0 \\ G - F_1\sin\beta - F_2\sin\alpha_A + T_{\mu1} + T_{\mu2} & = 0 \\ F_1\sin\beta + F_2\sin\alpha_A - \mathrm{Ma} + T_{\mu1} + T_{\mu2} & = 0 \\ K_2 L - F_2\cos\alpha_A & = 0 \end{cases} \tag{4}$$

Where $M$ is the mass of the WCRMP, and $L$ is the radial distance of the wheel.

## 3. Results

### 3.1 Mechanical Analysis of WCRMP

Considering that the aerodynamic flow field, formed by the high-speed rotation of twin propellers, will tilt the WCRMP; it is analysed, in order to eliminate the influence factors of the robot's adsorption instability. As shown in Fig. 10, when the airflow $v$ enters the left and right control frame, its entry speed is $v_c$, under the suction action of the brushless motor. If the adsorption of the WCRMP is stable at this time, the horizontal component of the airflow will completely disappear, when working, whereas only the reaction thrust remains to make the WCRMP, absorb to the wall smoothly.

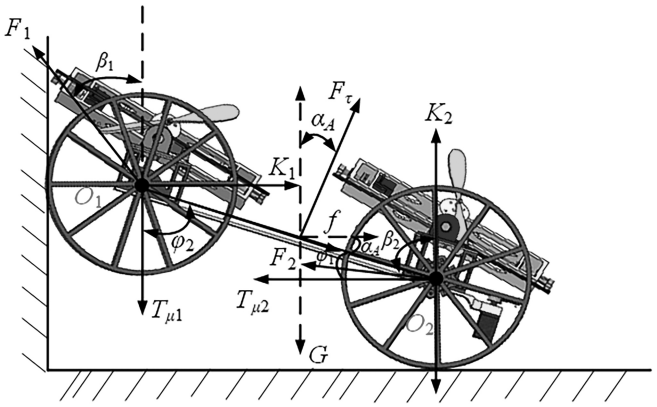


Figure 8. Force balance of the WCRMP in the critical state from ground to wall.

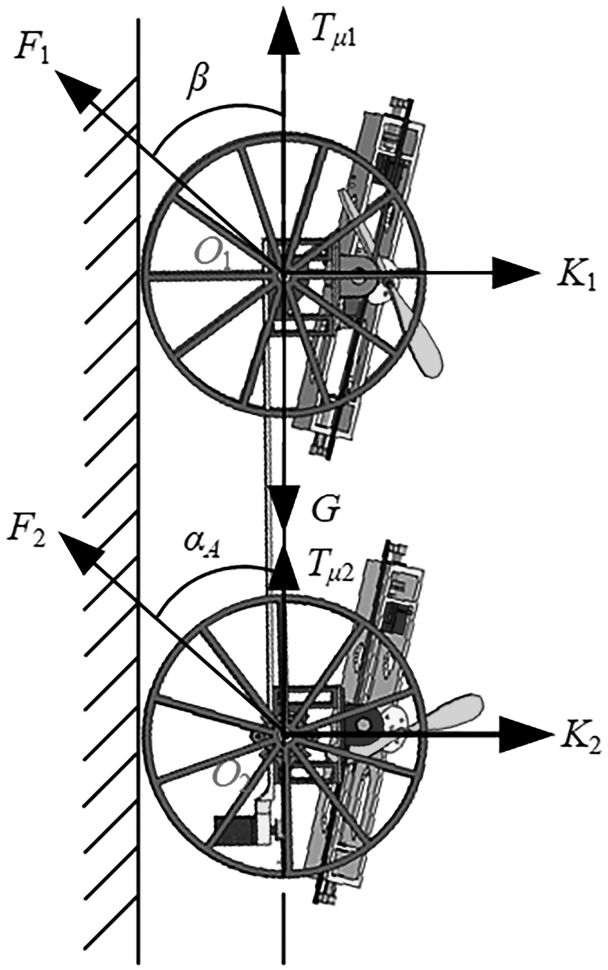


Figure 9. Force balance of the WCRMP in a corner.

The airflow effect, around the propeller, is analysed, using ANSYS software. The Euler model is adopted, setting the rotational speed at 500 rpm/s and the time step at 0.01. Figure 11 shows that, the speed changes in three directions $XYZ$. The brushless motor simulation demonstrates that the maximum value of the propeller is reached at some point after startup, the overall distribution trend is uniform and the lift power provided can also be used as the reverse thrust. When momentum is converted into energy, the

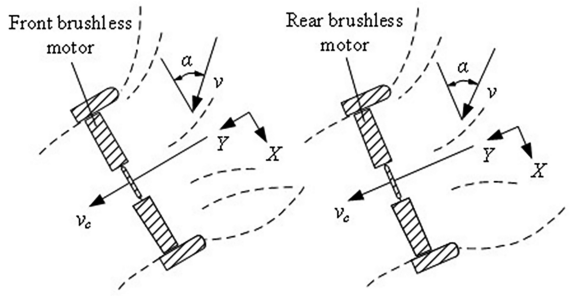


Figure 10. Schematic diagram of combined flow field from brushless motor and propeller suction.

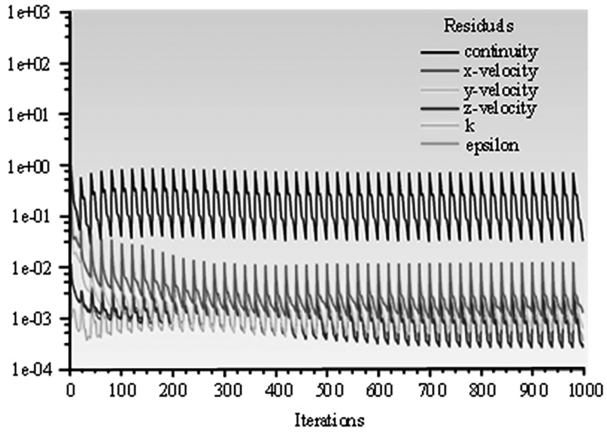


Figure 11. Simulation convergence diagram of ANSYS.

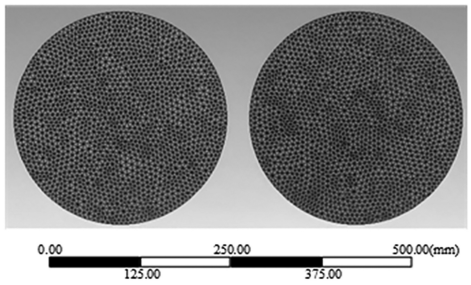


Figure 12. Grid diagram of propeller rotation domain.

brushless motor provides a flow opposite to the tension, in order to generate thrust.

### 3.2 Analysis of Adsorption Properties for Twin Propellers

The ANSYS fluent module is used to analyse and calculate the pressure generated by the twin propellers. The twin propellers model in the three-dimensional software CREO is imported and the unstructured mesh is used to divide the model. The simulation and test environments are ideal in open space, ignoring the influence of wind. The simulation geometry model parameters are introduced in Table 1.

When the clearance between propellers changes, different pressure distributions can be derived, according to the finite element grid diagram, generated by ANSYS,

Table 1
Geometric Parameters of the Simulation Model

| Parameters | Value |
|---|---|
| Relevance center | Fine |
| Model speed | 500 rpm/s |
| Air density | 1.229 kg/m$^3$ |
| Time step | 0.01 |
| Rotor disk diameter | 133 mm |
| Angle of rotor tilt | 0°–90° |
| Number of propellers | 2 |

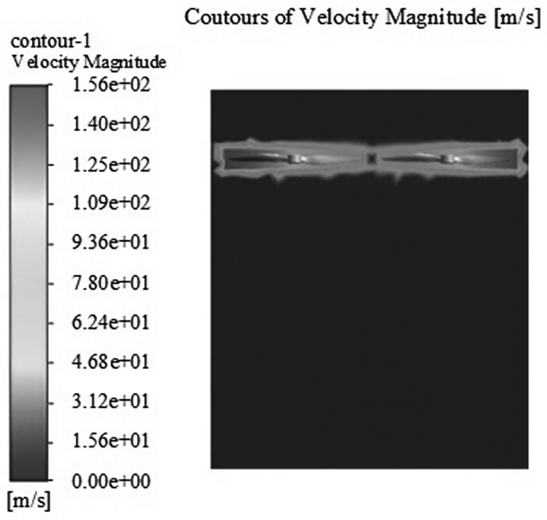


Figure 13. Cloud image of propeller velocity in the initial state.

as shown in Fig. 12. The gas flow in the propeller is a viscous type flow. As the Mach number at this position and the thickness of the viscous boundary layer, during normal operation, are different, the fluid pressure, corresponding to its thrust, is also different. Due to the viscosity effect, the tensile force changes, which affects the overall performance of the WCRMP.

In the brushless motor system, the additional tension of the brushless motor comes from the pressure difference between the low-pressure region and the high-pressure region, which is due to the change of the brushless motor's collecting flow. Due to the resistance moment of the brushless motor on the propeller, propeller tip vortices are suppressed and the viscous boundary layers in the culvert interfere violently with each other, which reduces the energy loss of the propeller wake and improves its linear thrust performance. Figure 13 shows the propeller velocity cloud diagram in the initial simulation state.

The airflow effect around the twin propellers is analysed in ANSYS, considering the velocity of the WCRMP at 500 rpm/s. As shown in Fig. 14, the

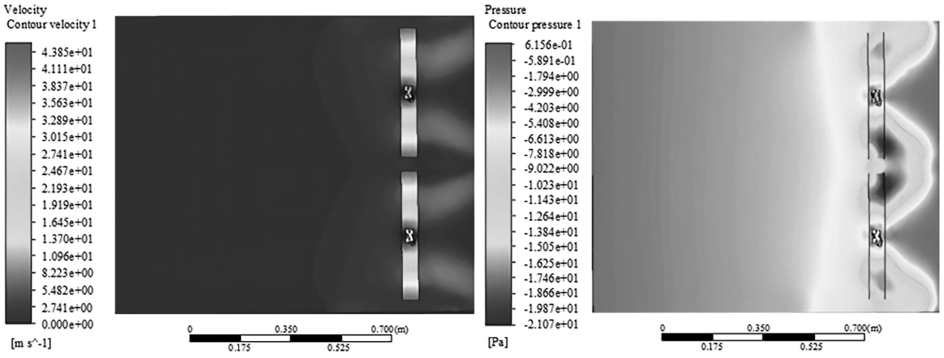


Figure 14. Cloud image of twin propeller velocity and pressure simulation.

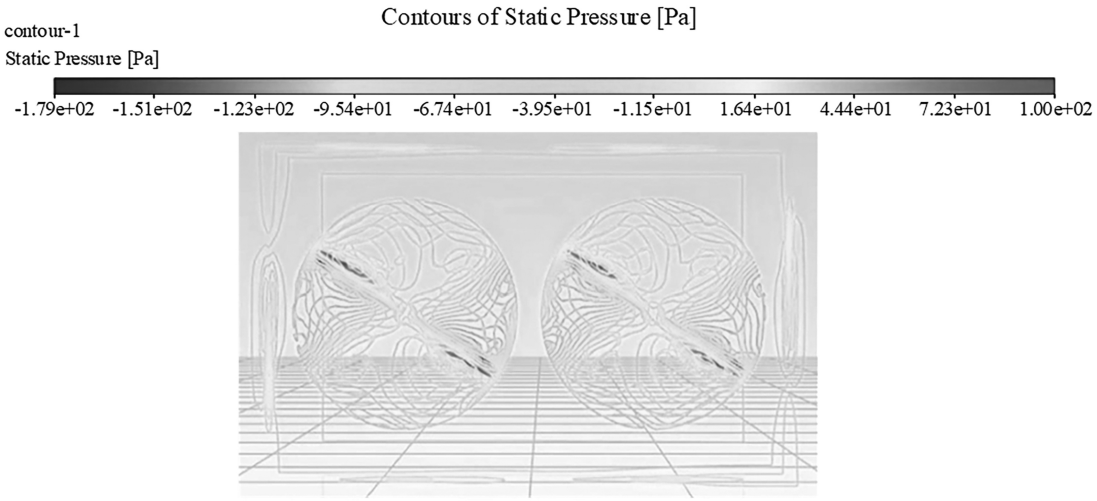


Figure 15. Pressure diagram of front and rear propeller rotation domain.

illustrated velocity and pressure cloud maps correspond to the twin propellers high speed rotation.

The force, as obtained during the rotation of the twin propellers, varies according to the position of the control frame. The streamline is set to 250, while the thrust inside and around its edge is analysed based on fluid simulation. The velocity flow, formed by the rotation of the propeller, runs into the inlet surface and is rapidly compressed by the twin propellers, to form a tension. The velocity flow runs out, through the outlet surface. The two rotation domains of the front and rear propellers of the WCRMP are obtained by using Boolean operation, as shown in Fig. 15. The maximum pressure of the propeller, in the rotation domain, is 100 Pa and the minimum is $-179$ Pa.

As shown in Fig. 16, the inclination angles of the twin propellers are set to 0°, 45°, 60°, and 90°, respectively. When the tilt angle of the propeller changes, the distance between the corresponding twin propellers axes also changes. As the tilt angle of the propeller increases, the distance between the two rotor shafts of the front and rear propeller gradually decreases. As shown in Fig. 16(a), when the rotor inclination angle of the current rear propeller is 0°, the distance between the corresponding rotor shafts is set at 500 mm and the rotor rotation axes are parallel. As shown in Fig. 16(d), when the rotor inclination angle of the front rear propeller is 90°, the rotation axes of the front and rear propeller rotors coincide. Figure 16 shows the velocity volume cloud image of the twin propellers of the WCRMP, at different inclination angles.

Under the control of the main control board, the front and rear propellers rotate counterclockwise. As the inclination angle rises, the air flow of the front propellers remains almost constant, whereas the rear propellers are affected by the front propellers. The airflow from the front propeller, flowing through the rear propeller, causes a pressure difference on the upper surface of the rear propeller, significantly reducing the adsorption force, generated by the propeller. As shown in Fig. 16(b) and (c), when the inclination angle of the front rotor is 45° and 60°, the wake direction of the front propeller changes, under the action of the rear propeller. As the propeller inclination angle increases, the adsorption force of the WCRMP gradually decreases.

## 4. Discussions

In order to verify the accuracy of the theoretical analysis and the function and effectiveness of the system, a prototype of the twin propellers WCRMP is developed, according to the proposed overall design

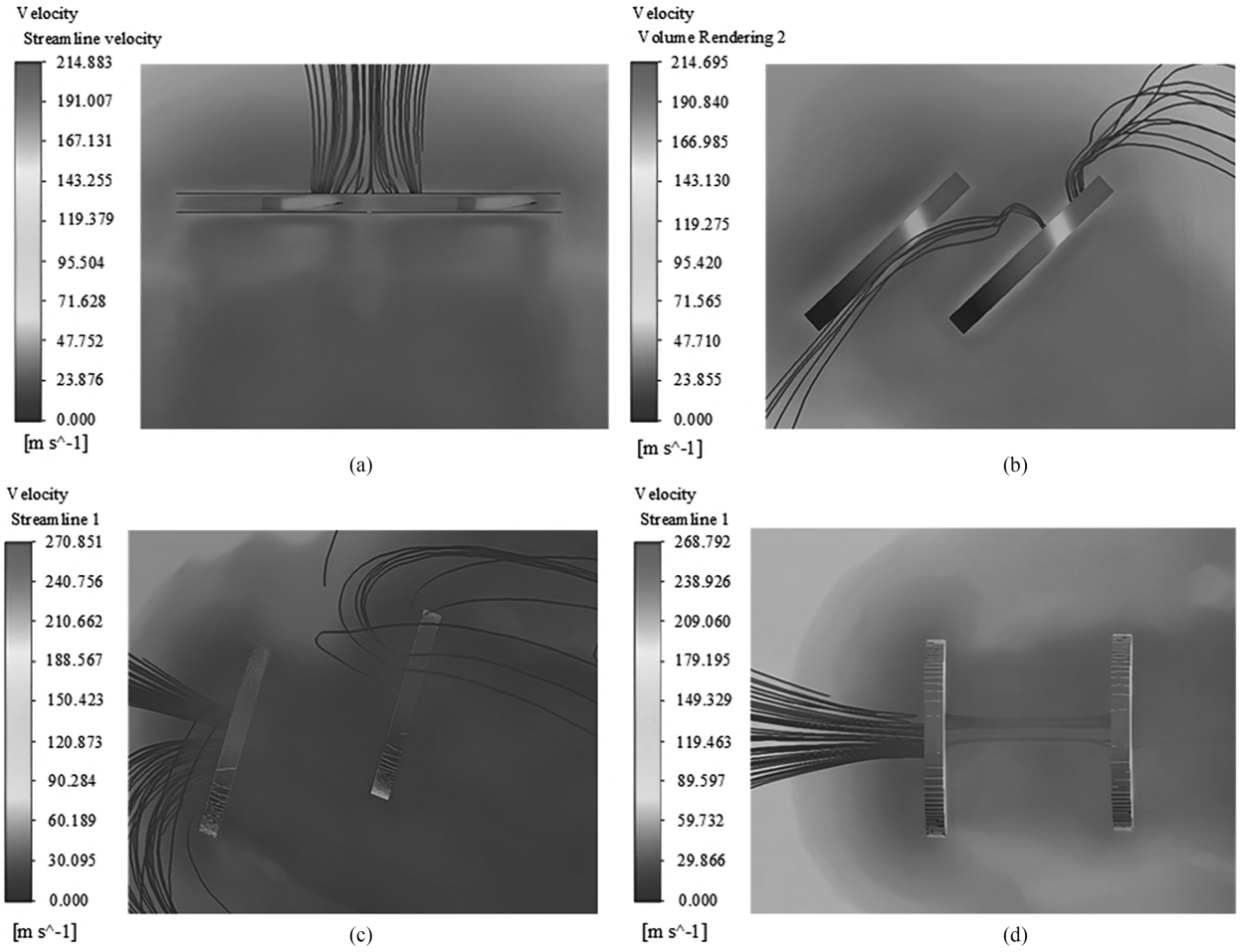


Figure 16. Volume velocity change in front and rear propeller rotation domain: (a) inclination angle of the twin propellers is 0°; (b) inclination angle of the twin propellers is 45°; (c) inclination angle of the twin propellers is 60°; and (d) inclination angle of the twin propellers is 90°.

scheme. The structure parameters of the WCRMP are shown in Table 2.

The controller is realised by using the Blinker app in the mobile phone, as shown in Fig. 17. It can control the Internet of Things devices through the mobile phone, mainly through Bluetooth, device sharing and speed switching.

Experiments are carried out on horizontal plane and inclined surface, at different angles, in order to analyse the drive control stability of the WCRMP in the cases of straight walking and turning motion. The WCRMP is able to move directly from the ground horizontal level to a sloping surface, at a small angle. When the inclination angle gradually increases, to a certain extent, the motion characteristics of the WCRMP will change, along with the adsorption and driving forces. The motion of the WCRMP on slopes of 30°, 45°, 60°, and 75° are illustrated in Fig. 18.

In order to measure the velocity of the WCRMP, a distance of 1 m and 2 m is set on the horizontal and vertical plane. The laser range finder (Victor 842B, Made in China) is used to measure the distance, and the infrared laser tachometer (Victor 6234P, Made in China) is used to measure the rotation speed of the WCRMP wheel to obtain the motion velocity, as shown in Fig. 19.

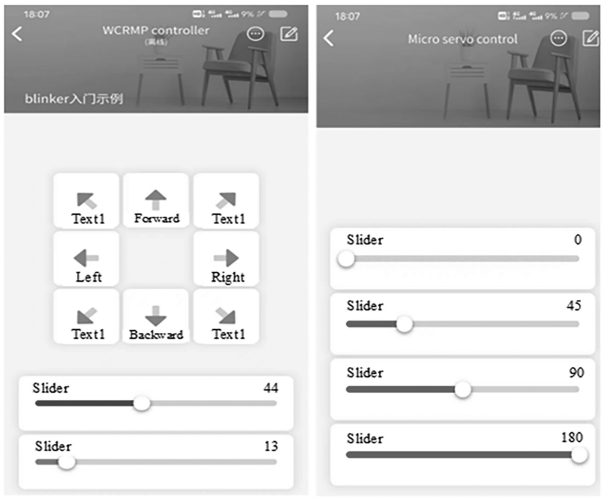


Figure 17. Mobile phone controller app Blinker.

A distance of 1 m and 2 m is set on the horizontal plane and vertical wall and each distance is measured 5 times. The velocity data obtained on the horizontal plane and on the vertical wall are shown in Tables 3 and 4. The

Table 2
The WCRMP structure parameters

| Objects | Parameter | Unit |
|---|---|---|
| Dimensions | 290×230×130 | mm |
| Overall weight | 0.9 | kg |
| Propeller thrust (max) | 1220 | G |
| Brushless DC motor | 400 | W |
| Battery | 11.1 | V |
| Propeller diameter | 153 | mm |
| Propeller number | 2 | — |
| Overall frame density (PLA printing) | 1230 | kg/m$^3$ |
| Micro servo | 4 (2 SG90 plastic, 2 MG996R metal) | — |
| Electronic speed controller | 20 | A |

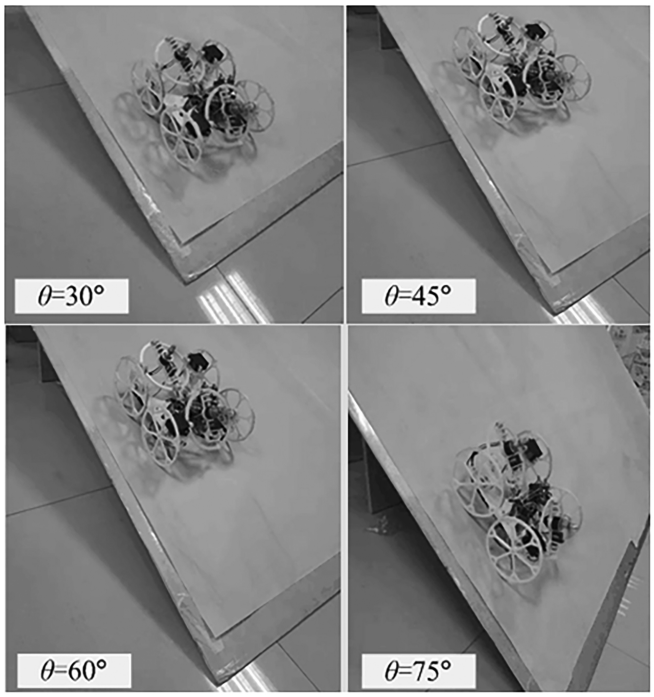


Figure 18. WCRMP motion on slopes of 30°, 45°, 60°, and 75°.

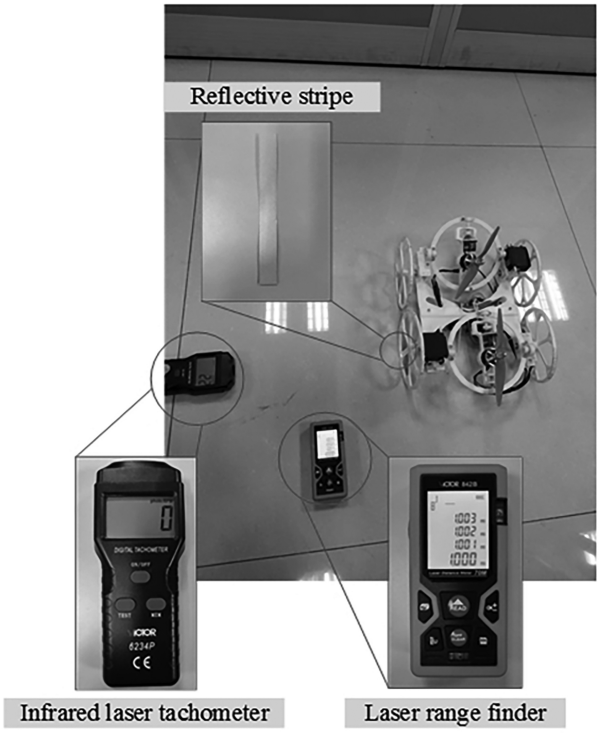


Figure 19. Measurement of WCRMP motion.

Table 3
Velocity Measurement of a WCRMP on the Horizontal Plane

| Distance (m) | Times | Rotation Speed (rpm) | Velocity (m/s) | Average Velocity (m/s) |
|---|---|---|---|---|
| 1 | 1 | 53 | 0.360 | 0.354 |
| | 2 | 51 | 0.347 | |
| | 3 | 54 | 0.367 | |
| | 4 | 55 | 0.354 | |
| | 5 | 50 | 0.340 | |
| 2 | 1 | 52 | 0.354 | 0.356 |
| | 2 | 52 | 0.354 | |
| | 3 | 51 | 0.347 | |
| | 4 | 53 | 0.360 | |
| | 5 | 54 | 0.367 | |

listings show that the average velocity along the 1 m and 2 m distance on the horizontal plane is 0.354 m/s and 0.351 m/s, respectively, while the average velocity along the 1 m and 2 m distance on the vertical wall is 0.075 m/s and 0.086 m/s, respectively.

To obtain the rotor reverse thrust, a thrust measuring device, including a force gauge (Victor 50, Made in China), a paddle, a brushless DC motor, an electronic speed controller, a signal receiver, and a lithium battery, is developed to measure the horizontal reverse thrust.

As shown in Table 5, with the increase of current, the reverse thrust also increases gradually. When the current is increased to 30 A, the maximum reverse thrust is 15.1 N. Therefore, the WCRMP can provide a reverse thrust of about 30 N.

Table 4
Velocity Measurement of a WCRMP on the Vertical Wall

| Distance (m) | Times | Rotation Speed (rpm) | Velocity (m/s) | Average Velocity (m/s) |
|---|---|---|---|---|
| 1 | 1 | 10 | 0.068 | 0.075 |
| | 2 | 11 | 0.075 | |
| | 3 | 9 | 0.061 | |
| | 4 | 12 | 0.082 | |
| | 5 | 13 | 0.088 | |
| 2 | 1 | 12 | 0.082 | 0.086 |
| | 2 | 10 | 0.068 | |
| | 3 | 13 | 0.088 | |
| | 4 | 14 | 0.095 | |
| | 5 | 14 | 0.095 | |

Table 5
Propeller Reverse Thrust Measurement

| Current (A) | 0 | 5 | 10 | 15 | 20 | 25 | 30 |
|---|---|---|---|---|---|---|---|
| Pull size (N) | 0 | 3.1 | 6.8 | 8.9 | 11.5 | 13.6 | 15.1 |

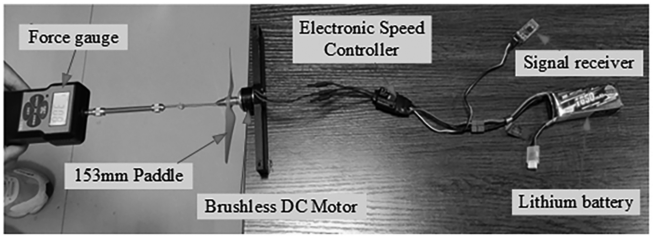


Figure 20. Tension measurement of WCRMP.

Table 6
The Roughness Values of Different Walls

| Materials | Painted Wall | Concrete Wall |
|---|---|---|
| Roughness ($\mu$m) | 2.853 | 6.168 |

The climbing motion experiment is carried out on a vertical wall and the WCRMP is controlled to move on a straight line on the wall, as shown in Fig. 21.

To test the WCRMP's wall adaptability, two different types of vertical walls (concrete wall and painted wall) are selected for testing, as shown in Fig. 22. The wall roughness data is shown in Table 6.

When the current is 20 A, WCRMP is compared and analysed in different concrete wall and painted wall from the aspects of roughness, thrust, and speed, as shown in Table 7. It can be seen that under the same current, the speed of the WCRMP is higher when the concrete

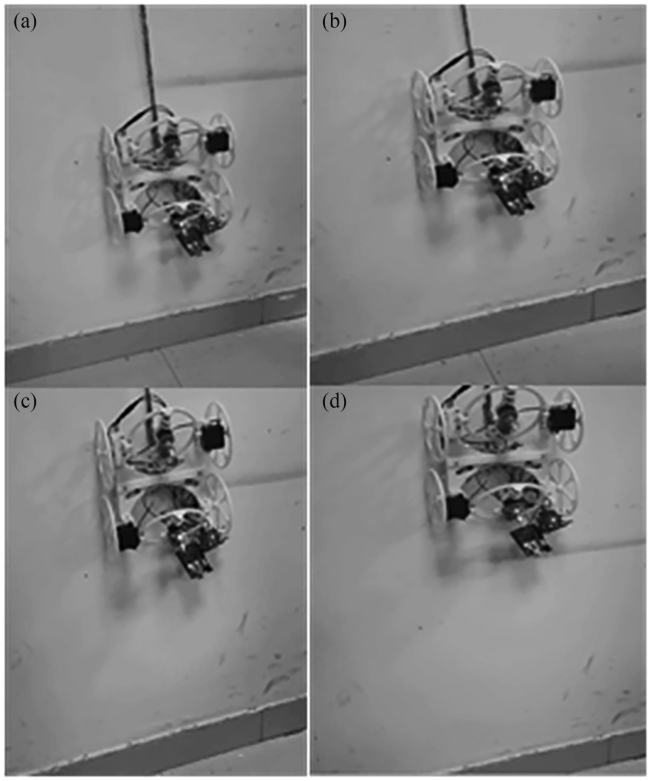


Figure 21. Wall climbing movement of WCRMP: (a) initial motion state; and (b)–(d) as the thrust increases, the WCRMP begins to move upward.

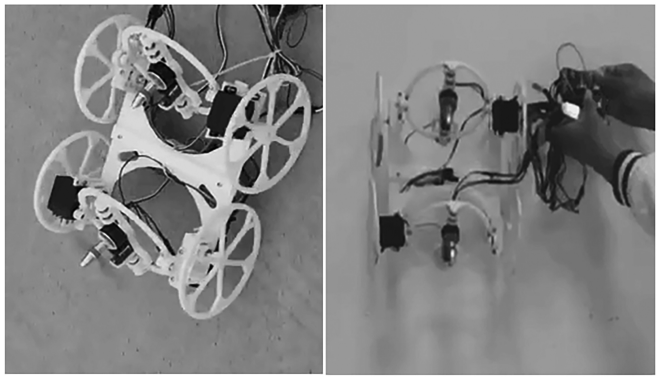


Figure 22. Experimental tests on walls with different roughnesses: (a) concrete wall and (b) painted wall.

Table 7
Comparative analysis of WCRMP on different walls

| Wall type Parameters | Pull Size (N) | Roughness ($\mu$m) | Velocity (m/s) |
|---|---|---|---|
| Concrete wall | 10.95 | 6.168 | 0.085 |
| Painted wall | 10.94 | 2.853 | 0.063 |

wall is applied than when the painted wall is applied. The reason is that the friction of the concrete wall is larger, the slip rate of the wheels is low, the thrust

loss provided by the propeller is less, and the movement efficiency of the WCRMP is high, which improves the moving speed.

## 5. Conclusion

In this paper, a multi-degree-of-freedom propeller WCRMP with reverse thrust adsorption is designed, developed, and tested. The static model is established and the velocity streamline of the propeller is analysed, using the momentum inflow model and blade element theory. The control mechanism of the WCRMP and the speed and pressure characteristics of the twin propellers are studied theoretically and experimentally. Based on the analysis of the static characteristics of the WCRMP, the kinematic balance relationship of the WCRMP motion, on the ground, during the ground-wall transition and on the wall, is obtained. The left and right control frames with multiple degrees of freedom are designed, so as to be able to adjust the fixed position of the brushless motor in the front and rear directions, followed by adjustment of the tension direction. The aerodynamic characteristics of the WCRMP system are analysed, using the momentum inflow model and the Euler force balance theorem, whereas the pressure distribution of the twin propellers is obtained. The maximum pressure in the propeller rotation domain is 100 Pa and the minimum value is –179 Pa. As the clearance between the propellers changes, different pressure distributions develop. In case the twin propellers rotate, the magnitude of the force varies, according to the position of the control frame. The change of inclination angle of the twin propellers of the WCRMP affects the adsorption force. The climbing experiment of the WCRMP on a small slope and the 90° stable adsorption experiment verify the feasibility of a stable robot motion on the vertical wall. The WCRMP can stably adsorb and move on the vertical wall.

## Acknowledgement

This work was supported by the Key Research Development and Promotion Special Project of Henan Province, under Grant 212102310119 and 212102210358, Scientific Research Foundation for High-level Talents of Henan Institute of Technology, under Grant KQ1869, University-Industry Collaborative Education Program, under Grant 202101187010 and 202102120046, Educational and Teaching Reform Research and Practice Project of Henan Institute of Technology, under Grant 2021-YB023 and JJXY-2021005, Innovative Education Curriculum Construction Project of Henan Institute of Technology, under Grant CX-2021-005, 2022 Xinxiang Federation of Social Sciences Research topic, under Grant SKL-2022-254 and SKL-2022-228, 2022 Annual Research Project of Henan Federation of Social Sciences: "Research on Rural Revitalization Strategy of Financial Service Model Innovation in Henan Province", under Grant SKL-2022-2692, Higher Education Teaching Reform Research and Practice Project of Henan Province, under Grant 2021SJGLX288 and 2021SJGLX289, Research and Practice Project of Research Teaching Reform in Henan University, under Grant 2022-YGZD01; and Innovation and entrepreneurship training program for college students in Henan Province, under Grant 202311329008.

## References

[1] A. Nishi, Y. Wakasugi, and K. Watanabe, Design of a robot capable of moving on a vertical wall, *Advanced Robotics*, *1*(1), 1986, 33–45.

[2] H.K. Beck, J.T. Schultz, and C.J. Clemente, A bio-inspired robotic climbing robot to understand kinematic and morphological determinants for an optimal climbing gait, *Bioinspiration and Biomimetics*, *17*(1), 2021, 016005.

[3] Y. Fang, S. Wang, Q. Bi, D. Cui, and C. Yan, Design and technical development of wall-climbing robots: A review, *Journal of Bionic Engineering*, *19*(4), 2022, 877–901.

[4] S. Nansai and R.E. Mohan, A survey of wall climbing robots: Recent advances and challenges, *Robotics*, *5*(3), 2016, 14.

[5] P. Chattopadhyay and S.K. Ghoshal, Adhesion technologies of bio-inspired climbing robots: A survey, *International Journal of Robotics and Automation*, *33*(6), 2018, 654–661.

[6] T.W. Seo, Y. Jeon, C. Park, and J. Kim, Survey on glass and façade-cleaning robots: Climbing mechanisms cleaning methods and applications, *International Journal of Precision Engineering and Manufacturing-Green Technology*, *6*(2), 2019, 367–376.

[7] H.A. Kazem, M.T. Chaichan, A.H. Al-Waeli, and K. Sopian, A review of dust accumulation and cleaning methods for solar photovoltaic systems, *Journal of Cleaner Production*, *276*, 2020, 123187.

[8] M.A. Viraj, M. Muthugala, M. Rajesh Elara, and R. Suresh, Design and control of a wall cleaning robot with adhesion-awareness, *Symmetry*, *12*(1), 2020, 1–18.

[9] M. Rostami and A. H. Farajollahi, Aerodynamic performance of mutual interaction tandem propellers with ducted UAV, *Aerospace Science and Technology*, *108*, 2021, 106399.

[10] J. Jose, D. Devaraj, R.M. Mathanagopal, K.C. Ramanathan, M.O. Tokhi, and T.P. Sattar, Investigations on the effect of wall thickness on magnetic adhesion for wall climbing robots, *International Journal of Robotics and Automation*, *36*(4), 2020, 1–8.

[11] W.R. Provancher, S.I. Jensen-Segal, and M.A. Fehlberg, ROCR: An energy-efficient dynamic wall-climbing robot, *IEEE/ASME Transactions on Mechatronics*, *16*(5), 2010, 897–906.

[12] K. Carpenter, N. Wiltsie, and A. Parness, Rotary microspine rough surface mobility, *IEEE/ASME Transactions on Mechatronics*, *21*(5), 2015, 2378–2390.

[13] H. Li, X. Sun, Z. Chen, L. Zhang, H. Wang, and X. Wu, Design of a wheeled wall climbing robot based on the performance of bio-inspired dry adhesive material, *Robotica*, *40*(3), 2022, 611–624.

[14] W. Wang, B. Tang, H. Zhang, and G. Zong, Robotic cleaning system for glass facade of high–rise airport control tower, *Industrial Robot: An International Journal*, *37*(5), 2010, 469–478.

[15] Z. Qian, Y. Zhao, and Z. Fu, Development of wall-climbing robots with sliding suction cups, *Proc. 2006 IEEE/RSJ International Conf. on Intelligent Robots and Systems*, Beijing, 2006, 3417–3422.

[16] R.S. Bisht, P.M. Pathak, and S.K. Panigrahi, Design and development of a glass façade cleaning robot, *Mechanism and Machine Theory*, *168*, 2022, 104585.

[17] A.A. Kumar, R.K. Akhil, A.A. Ajnas, E.V. Abdul Vasih, and J. Jithu, Modelling and simulation of semi-automatic glass window cleaning machine, *IOP Conference Series: Materials Science and Engineering*, *1114*(1), 2021, 012057.

[18] K. Shi and X. Li, Vacuum suction unit based on the zero pressure difference method, *Physics of Fluids*, *32*(1), 2020, 017104.

[19] F. Zhang, X. Sun, Z. Li, I. Mohsin, Y. Wei, and K. He, Influence of processing parameters on coating removal for high pressure

water jet technology based on wall-climbing robot, *Applied Sciences*, *10*(5), 2020, 1862.
[20] Z. Zhao, Y. Tao, J. Wang, and J. Hu, The multi-objective optimization design for the magnetic adsorption unit of wall-climbing robot, *Journal of Mechanical Science and Technology*, *36*(1), 2022, 305–316.
[21] J. Fan, T. Xu, Q. Fang, J. Zhao, and Y. Zhu, A novel style design of a permanent-magnetic adsorption mechanism for a wall-climbing robot, *Journal of Mechanisms and Robotics*, *12*(3), 2020, 035001.
[22] S.Y. Bian, Y.L. Wei, F. Xu, and D.Y. Kong, A fourlegged wall-climbing robot with spines and miniature setae array inspired by longicorn and gecko, *Journal of Bionic Engineering*, *18*, 2021, 292–305.
[23] A.G. Dharmawan, P. Xavier, H.H. Hariri, G.S. Soh, A. Baji, R. Bouffanais, S. Foong, H.Y. Low, and K.L. Wood, Design, modeling, and experimentation of a bio-inspired miniature climbing robot with bilayer dry adhesives, *Journal of Mechanisms and Robotics–Transactions of the ASME*, *11*, 2019, 020902.
[24] Y. Liu, L. Wang, S. Liu, T. Mei, P. Li, and Y. Li, Design and analysis of an inchworm-inspired wall-climbing robot, *Journal of Mechanical Transmission*, *43*(8), 2019, 87–91.
[25] P. Liang, X. Gao, Q. Zhang, M. Li, R. Gao, and Y. Xu, Analysis and experimental research on motion stability of wall-climbing robot with double propellers, *Advances in Mechanical Engineering*, *13*(9), 2021, 1–13.
[26] P. Liang, X. Gao, Q. Zhang, R. Gao, M. Li, Y. Xu, and W. Zhu, Design and stability analysis of a wall-climbing robot using propulsive force of propeller, *Symmetry*, *13*(1), 2021, 1–13.
[27] S.K. Mahmood, S.H. Bakhy, and M.A. Tawfik, Propeller-type wall-climbing robots: A review, *IOP Conference Series: Materials Science and Engineering*, *1094*(1), 2021, 012106.
[28] M.A. Fanni, M.G. Alkalla, and A. Mohamed, Propeller type skid steering climbing robot based on a hybrid actuation system, *International Journal of Robotics and Automation*, *33*(3), 2018, 1–20.
[29] M. Li, X. Gao, Q. Zhang, P. Liang, Y. Wei, and K. Li, Force analysis and verification of wall-climbing robot with rotor-propellers, *Proc. 2022 IEEE International Conf. on Mechatronics and Automation (ICMA)*, Guilin, 2022, 1171–1177.
[30] Y. Wei, Q. Zhang, X. Gao, P. Liang, M. Li, and K. Li, Aerodynamic analysis of a wall-climbing robot with dual-propeller, *Proc. 2022 IEEE International Conf. on Mechatronics and Automation (ICMA)*, Guilin, 2022, 1537–1542.
[31] A. Bhaskar, G. Verma, and S. Sharma, MARVEL: A high pitch agile bi-copter wall-climbing robot, *Proc. Advances in Robotics-5th International Conf. of The Robotics Society*, Kanpur, 2021, 1–6.

## Biographies

*Minglu Chi* received the Ph.D. degree in mechanical engineering from the Key Laboratory of Technology Precision and Non-Traditional Machining, Ministry of Education, Dalian University of Technology, in 2018. He is currently an Associate Professor with the School of Intelligent Engineering, Henan Institute of Technology. He has been involved two research projects of the National Natural Science Foundation of China. He is the author of several papers and patents. His current research interests include dynamics of micromedical robots and magnetic control technology.

*Shuaibing Chang* received the B.S. degree in information and computational science from Hebei University of Science and Technology in 2009, and the M.S. degree in applied mathematics from Hebei University of Science and Technology in 2012, and the Ph.D. degree in control theory and control engineering from North China Electric Power University in 2018. He is currently a Lecturer with the School of Electrical Engineering, Henan Institute of Technology. His current research interests include power system load frequency control, intelligent optimisation control and intelligent algorithm, and high voltage and new energy power generation technology.

*Fuchao Yang* received the M.S. degree from Henan Polytechnic University, in 2008. His current research interests include motion control of industrial robots.

*Xiaoyan Qian* received the M.S. degree from the Inner Mongolia Agricultural University, in 2013. Her current research interests include intelligent irrigation system.

*Shuaihua Cui* received the M.S. degree from Henan Polytechnic University, in 2021. His current research interests include computer vision and deep learning.

*Jinzhan Wang* is currently pursuing the undergraduation degree with the School of Intelligent Engineering, Henan Institute of Technology. His research interest is motion control algorithm for wall-climbing robot.

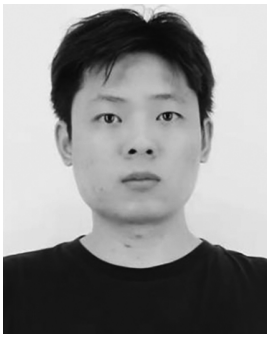

*Lun Zhao* received the B.S. degree in robot engineering from the School of Intelligent Engineering, Henan Institute of Technology, in 2023. His research interests are kinematics of wall-climbing robot and visual detection of wall damage.

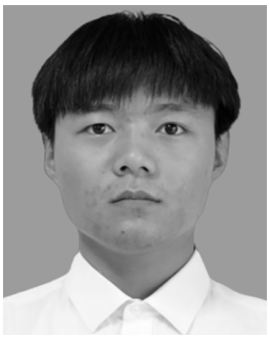

*Ruihua Ren* received the B.S. degree in robot engineering from the School of Intelligent Engineering, Henan Institute of Technology, in 2022. His research interests are wall-climbing robot and pipe robot.